

MID-INFRARED IRS SPECTROSCOPY OF NGC 7331: A FIRST LOOK AT THE SINGS LEGACY

J.D.T. SMITH¹, D.A. DALE², L. ARMUS³, B.T. DRAINE⁴, D.J. HOLLENBACH⁵, H. ROUSSEL⁶, G. HELOU⁶, R.C. KENNICUTT, JR.¹, A. LI¹, G.J. BENDO¹, D. CALZETTI⁷, C.W. ENGELBRACHT¹, K.D. GORDON¹, T.H. JARRETT⁶, L. KEWLEY⁹, C. LEITHERER⁷, S. MALHOTRA⁷, M.J. MEYER⁷, E.J. MURPHY⁸, M.W. REGAN⁷, G.H. RIEKE¹, M.J. RIEKE¹, M.D. THORNLEY^{10,7}, F. WALTER¹¹, AND M.G. WOLFIRE¹²

Draft version June 12, 2018

ABSTRACT

The nearby spiral galaxy NGC 7331 was spectrally mapped from 5–38 μm using all modules of *Spitzer*'s IRS spectrograph. A strong new dust emission feature, presumed due to PAHs, was discovered at 17.1 μm . The feature's intensity is nearly half that of the ubiquitous 11.3 μm band. The 7–14 μm spectral maps revealed significant variation in the 7.7 and 11.3 μm PAH features between the stellar ring and nucleus. Weak [O IV] 25.9 μm line emission was found to be centrally concentrated in the nucleus, with an observed strength over 10% of the combined neon line flux, indicating an AGN or unusually active massive star photo-ionization. Two [S III] lines fix the characteristic electron density in the H II regions at $n_e \lesssim 200 \text{ cm}^{-3}$. Three detected H₂ rotational lines, tracing warm molecular gas, together with the observed IR continuum, are difficult to match with standard PDR models. Either additional PDR heating or shocks are required to simultaneously match lines and continuum.

Subject headings: galaxies: individual (NGC 7331) – galaxies: ISM – dust, extinction – infrared: galaxies – techniques: spectroscopic – lines: identification

1. INTRODUCTION

The mid-infrared (MIR) spectra of star-forming galaxies are characterized by fine structure and molecular hydrogen lines, and broad emission features usually attributed to the large molecular polycyclic aromatic hydrocarbon (PAH) species, set against a continuum transitioning from the direct photospheric emission of cool stars at short wavelengths to the rapidly rising contribution from very small grains and heated dust toward longer wavelengths. The Infrared Space Observatory (ISO) revolutionized the use of both line and band features in the MIR as diagnostics of star-formation and AGN activity in galaxies dominated by infrared emission, and found several key relationships between lines that trace excitation and the hardness of the ultraviolet radiation field (e.g. [Ne III]/[Ne II], Thornley et al. 2000), star-formation (e.g. 7.7 μm PAH, Genzel et al. 1998) and active nuclei (e.g. [Ne V] & [O IV], Sturm et al. 2002).

The *Spitzer Space Telescope* offers for the first time the sensitivity and spatial resolution necessary to apply the suite of infrared diagnostics to individual environments in galaxies which span a full range of interstellar medium (ISM) and IR emission properties. This is the focus of the *Spitzer* Infrared Nearby Galaxies Survey (SINGS — Kennicutt et al. 2003, hereafter K03), a

Legacy program for which NGC 7331 is the first galaxy observed by *Spitzer*.

NGC 7331 has an IR luminosity typical of normal spiral galaxies with moderate star-formation activity, with an IR to optical ratio $L_{\text{IR}}/L_{\text{opt}} \sim 1$. By comparison, the extreme starburst M82 has $L_{\text{IR}}/L_{\text{opt}} \sim 40$, and ultra-luminous infrared galaxies range in IR activity up to ~ 400 (Sanders & Mirabel 1996). Kinematic and high-resolution studies in both the optical and radio have been unable to determine whether the galaxy harbors an AGN (e.g. Filho et al. 2002).

ISO imaging of NGC 7331 was obtained by Smith (1998), who found little variation in the coarse MIR spectral energy distribution traced in six broad bandpasses from 6–15 μm , three of which roughly match prominent PAH features. A surprising result from ISO was that the 2.5–11.6 μm spectral shape is relatively invariant among normal galaxies, with the appealing explanation that the PAH molecules whose features dominate this wavelength region are transiently heated by single photons, and thus produce an emission spectrum roughly independent of the heating environment (Helou et al. 2001). The spectral mapping capabilities of *Spitzer* make it possible to investigate variations in the PAH emission spectrum *within* individual galactic environments, and couple these variations using fine structure and molecular lines to the physical parameters of the ISM, H II and photo-dissociation regions (PDRs).

2. OBSERVATIONS AND REDUCTION

Spectra were obtained using all four modules of the Infrared Spectrograph (IRS, Houck et al. 2004) in *Spectral Mapping Mode*. In this mode, the spacecraft moves in a rectangular raster of discrete steps, settling at each position before the integrations begin. For all maps, half-slit step sizes were used. Since *Spitzer* cannot roll to alter the position angle of the slits, the mapping strategy was designed to provide the maximum useful overlap be-

¹ Steward Observatory, University of Arizona, Tucson, AZ 85721

² Physics & Astronomy, Univ. of WY, Laramie, WY 82071

³ Spitzer Science Center, Caltech, Pasadena, CA 91125

⁴ Princeton University Observatory, Princeton, NJ 08544

⁵ NASA Ames Research Center, Moffett Field, CA 94035

⁶ Caltech, Pasadena, CA 91101

⁷ STScI, Baltimore, MD 21218

⁸ Dept. of Astronomy, Yale University, New Haven, CT 06520

⁹ Harvard-Smithsonian CfA, Cambridge, MA 02138

¹⁰ Dept. of Physics, Bucknell University, Lewisburg, PA 17837

¹¹ NRAO, PO Box O, Socorro, NM 87801

¹² Astronomy Dept., Univ. of MD, College Park, MD 20742

Electronic address: jdsmith@as.arizona.edu

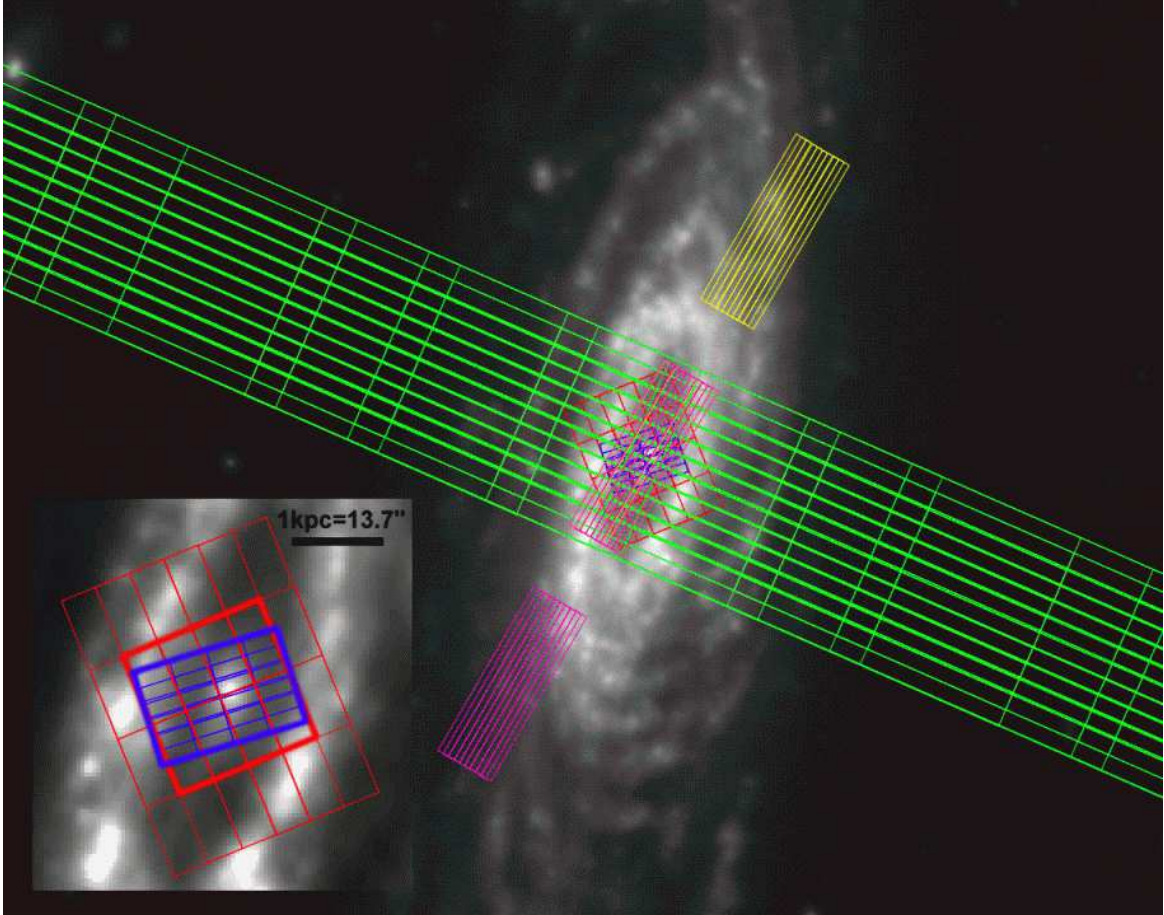


FIG. 1.— An overlay of the IRS footprints on the $8\,\mu\text{m}$ IRAC image, with the nucleus magnified inset, highlighting the corresponding apertures used in LH ($19\text{--}37\,\mu\text{m}$, red) and SH ($10\text{--}20\,\mu\text{m}$, blue). The $14\text{--}38\,\mu\text{m}$ LL radial strip is in green (atypically, following the minor axis due to unusual scheduling constraints for this galaxy), while the SL $5\text{--}14\,\mu\text{m}$ regions covered are in magenta and yellow (composed of two subslits, with the central area mapped in both subslits). The distance of NGC 7331 is 15.1 Mpc ($1\text{ kpc} = 13.66''$).

tween modules. Figure 1 illustrates these areas overlaid on a SINGS $8\mu\text{m}$ IRAC image (see Regan et al. 2004, in this volume), and indicates the high-resolution apertures used for computing line parameters.

Integration times ranged from 14–60s per pointing, with each position covered 2–4 times, matching the uniform SINGS observational strategy outlined in K03. The two IRS low-resolution modules, short-low (SL, $5\text{--}14\mu\text{m}$) and long-low (LL, $14\text{--}38\mu\text{m}$), provide $R=50\text{--}100$, while the two high-resolution modules, short-high (SH, $10\text{--}20\mu\text{m}$) and long-high (LH, $19\text{--}38\mu\text{m}$), deliver $R\sim 600$.

The individual low-res spectra from each map were assembled into spectral cubes by CUBISM (see K03, §6.2), which was also used to produce maps and extract spectra. The pipeline and calibration products used were version S9.5.0. Low-resolution spectra were flux-calibrated using the standard IRS FLUXCON tables (see Spitzer Observer’s Manual¹³, Chap. 7), which provide unbiased fluxes only for point sources. We derived extended source flux intensities by applying three corrections: 1) an empirically determined *aperture loss correction function* which accounts for the pipeline’s narrowing, point-source specific extraction aperture, 2) an estimate of the *slit loss correction function* which results from the point-spread function over-filling the IRS slits, and 3) an estimate of the integrated cross-slit beam profile. The LL background was subtracted *in situ* using the extended off-source map wings, and the SL background was fit and removed using two off-source spectra. High-resolution spectra were extracted directly from pre-flatfield data and flux calibrated using stellar standards via an empirically derived relative spectral response function. This resulted in an absolute calibration accuracy of 25%.

3. RESULTS

3.1. The Spatially Varying PAH Spectrum and a Broad $17\mu\text{m}$ Feature

The entire $5\text{--}38\mu\text{m}$ low-resolution spectrum extracted from a $58''\times 17''$ region, covering both the nucleus and a portion of the ring, is shown in Fig. 2. Most of the fine structure and H_2 lines are detected in the low-resolution spectrum. The complete PAH spectrum from $5\text{--}20\mu\text{m}$ is inset, with an untailored diffuse ISM PAH + graphite + silicate model of Li & Draine (2001) overlaid. The model matches the four main PAH bands, at 6.2 , 7.7 , 8.6 , and $11.3\mu\text{m}$, reasonably well. The feature at $12.7\mu\text{m}$ is contaminated by $[\text{Ne II}]$ $12.8\mu\text{m}$, but is also in good agreement with the model when the $[\text{Ne II}]$ line flux is considered. Broad $10\mu\text{m}$ silicate absorption is likely present, as the continuum between $7.7\mu\text{m}$ and $11.3\mu\text{m}$ features lies below that inferred from bracketing band-free regions, most easily seen in the strong departure from the scaled model in this region.

Of particular interest is the bright, broad complex at $17\mu\text{m}$, blended with $\text{H}_2\text{S}(1)$. The PAH model reproduces the narrow peak on the blue wing of the feature, but does not predict the large width observed, which is approximately equal to that of the $7.7\mu\text{m}$ PAH band. Further peaks modeled at 18 and $21\mu\text{m}$ are not evident in the spectra. Deuterated PAHs are expected to have C-D out-of-plane bending modes which emit in the $14\text{--}16\mu\text{m}$ region, but the observed $17\mu\text{m}$ feature falls longward of

these and is *much* stronger. It may be due to PAH C-C-C bending modes (e.g. Allamandola & Hudgins 2003).

Moutou et al. (2000) found a strong, narrow but resolved emission feature at $16.4\mu\text{m}$ in ISO SWS spectra of the bright reflection nebula NGC 7023, the Orion bar, and on the surface of a Galactic molecular cloud. Their spectra showed no other features between 15.2 and $17.2\mu\text{m}$. IRS spectra of NGC 7023 reveal a series of blended peaks at 16.4 , 17.4 , and $17.8\mu\text{m}$ which vary strongly across the nebula (see Werner et al. 2004, in this volume). NGC 7331 is the first extragalactic source in which this feature has been discovered.

In Fig. 3, we fit the blended $17\mu\text{m}$ feature as a combination of three unresolved lines matching SH identifications, and two PAH bands — one as previously reported at $16.4\mu\text{m}$, and a new, much stronger feature at $17.1\mu\text{m}$. Removing the line contaminants, the combined $16.4 + 17.1\mu\text{m}$ feature strength is $1.5 \times 10^{-7} \text{ W m}^{-2} \text{ sr}^{-1}$, fully 49% of the $11.3\mu\text{m}$ feature strength, making it a potentially important contributor to the total MIR luminosity, and a necessary consideration in the interpretation of photometric redshift and luminosity distributions based on $24\mu\text{m}$ MIPS or longer imaging.

Using the MIR spectral cubes, we can test the spatial variability of PAH emission on kiloparsec scales. Figure 4 illustrates three maps created from the SL spectral cube. The topmost map (red) is a combination of the 7.7 , 8.6 , 11.3 , and $12.7\mu\text{m}$ PAH features (as indicated by shading on the spectra at right), and highlights the mapped portion of the ring and resolved nuclear core. In the continuum-subtracted $7.7\mu\text{m}$ map (green, at middle), the nucleus, with its weak $7.7\mu\text{m}$ PAH feature, nearly vanishes. In the pure continuum map at $10\mu\text{m}$ (blue, at bottom), the strong inter-feature continuum of the nuclear emission is demonstrated. The three spectra extracted from ring, nucleus, and both components together, illustrate the spatial variability of the relative $7.7\mu\text{m}$ and $11.3\mu\text{m}$ PAH strengths. Although the apparent strength of the nuclear $7.7\mu\text{m}$ PAH feature is diluted by excess continuum, the $7.7\mu\text{m}/11.3\mu\text{m}$ ratio increases by $\sim 40\%$ from nucleus to ring. A similar band ratio increase, correlated with increasing star formation activity, has also been observed in M31 (Pagani et al. 1999).

3.2. H_2 and Fine Structure Line Emission

We detected seven fine structure and three molecular hydrogen lines, averaged over areas of size $22''\times 22.4''$ (LH) and $23.1''\times 15.7''$ (SH) ($\sim 1\text{--}1.5\text{ kpc}$ on a side at the 15.1 Mpc distance of NGC 7331, see Fig. 1 inset). The fine structure lines detected arise from species ranging in ionization potential from 8.2 eV (Si^+) to 55 eV (O^{3+}). The line parameters are given in Table 1, and individual line cut-outs are shown in Fig. 5.

The $18.71\mu\text{m}$ and $33.48\mu\text{m}$ fine structure lines of $[\text{S III}]$ are detected. For $T \sim 8000\text{ K}$ the $[\text{S III}]$ $18.71\mu\text{m}/[\text{S III}]$ $33.48\mu\text{m}$ line ratio is insensitive to temperature and provides a density diagnostic. The density obtained with this diagnostic is $n_e \lesssim 200\text{ cm}^{-3}$. This density corresponds to a thermal pressure $p/k \lesssim 4 \times 10^6\text{ cm}^{-3}\text{ K}$ in the H II regions.

The pure rotational lines of molecular hydrogen, especially the $\text{S}(1)$ and $\text{S}(2)$ lines, which require $T \gtrsim 100\text{ K}$ for excitation, likely arise in PDRs surrounding or adjacent to these H II regions, and can be used to provide joint

¹³ <http://ssc.spitzer.caltech.edu/documents/som/>

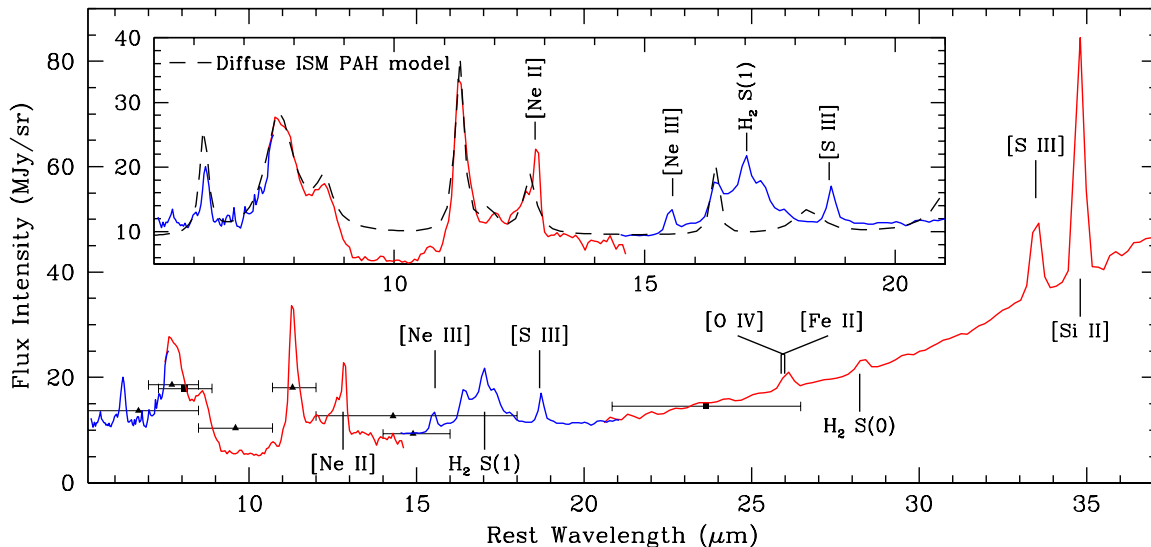


FIG. 2.— The low-resolution spectrum of the inner ring and nucleus (central magenta rectangle in Fig. 1). Alternating colors indicate spectra from the four SL and LL orders. Inset, the expanded PAH spectrum with a diffuse ISM PAH + graphite + silicate model (Li & Draine 2001) overlaid as a dashed line, arbitrarily scaled to match the $7.7\,\mu\text{m}$ peak. The broad $17\,\mu\text{m}$ complex seen is blended with $\text{H}_2\text{ S}(1)$, and contains a sharp feature matching the model at $16.4\,\mu\text{m}$. Filled points represent matched photometry with filter widths shown, where squares denote IRAC $8\,\mu\text{m}$ and MIPS $24\,\mu\text{m}$ (Regan et al. 2004), and triangles denote ISOCAM LW2 ($5.0\,\mu\text{m}$), LW6 ($7.0\,\mu\text{m}$), LW7 ($8.5\,\mu\text{m}$), LW8 ($10.7\,\mu\text{m}$), LW3 ($12.0\,\mu\text{m}$), and LW9 ($14.0\,\mu\text{m}$).

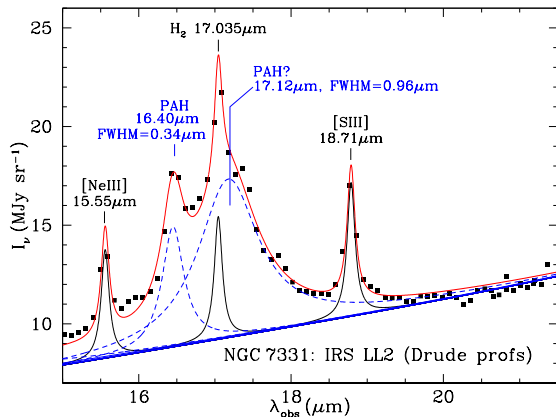


FIG. 3.— A fit to the $17\,\mu\text{m}$ feature, including unresolved $[\text{Ne III}]$, $[\text{S III}]$, and $\text{H}_2\text{ S}(1)$ in black, as well as two Drude-profile PAH components in blue: the previously discovered $16.4\,\mu\text{m}$ feature, and a new, much stronger $17.1\,\mu\text{m}$ band.

constraints on the pressure or density and starlight intensity there. The observed $\text{H}_2\text{ S}(0)/\text{S}(1)$ and $\text{S}(1)/\text{S}(2)$ line ratios and intensities can be reproduced by PDR models (Draine & Bertoldi 2001, M.J. Kaufman et al. 2004, in prep.) with a large fraction of PDRs in the beam having a similar thermal pressure as the ionized gas, typically $T \sim 500\text{ K}$ and $n \sim 5000\text{ cm}^{-3}$ at the surface, with incident FUV fluxes roughly $G_0 \gtrsim 10^2$ times the local interstellar value. This is consistent with the strong $20\text{--}37\,\mu\text{m}$ continuum observed in Fig. 2, which indicates a component of dust with temperature $30\text{--}60\text{ K}$; such warm dust requires $G_0 \sim 10^2\text{--}10^3$.

The nucleus and inner edge of the circumnuclear ring in NGC 7331 therefore appear dominated by H II regions and PDRs. However, our current PDR models tend to create too much warm dust for the observed $30\,\mu\text{m}$ continuum. This may indicate either a lack of understand-

TABLE 1
OBSERVED LINE PARAMETERS

Line	λ_{rest} μm	Flux Intensity		I.P. or $\Delta E/k^c$
		Inner ^a 10^{-10}	Outer ^b $\text{W m}^{-2} \text{ sr}^{-1}$	
Fine Structure				
[Ne II]	12.81	237.2 ± 8.3	...	21.6 eV
[Ne III]	15.56	164.7 ± 7.5	...	41.1 eV
[S III]	18.68	100.7 ± 15.1	...	23.4 eV
[O IV]	25.89	39.6 ± 5.5	16.2 ± 4.4	54.9 eV
[Fe II]	25.99	36.7 ± 11.0	29.2 ± 1.8	7.9 eV
[S III]	33.48	189.5 ± 19.7	251.3 ± 19.7	23.4 eV
[Si II]	34.82	463.1 ± 49.1	585.9 ± 38.1	8.2 eV
Molecular Hydrogen				
H ₂ S(2)	12.28	43.8 ± 14.7	...	1682 K
H ₂ S(1)	17.04	108.0 ± 7.5	...	1015 K
H ₂ S(0)	28.22	34.2 ± 5.9	43.3 ± 6.2	510 K

^aAverage intensity over $\sim 22''$ region as indicated in Fig. 1

^bWeighted average intensity over the entire LH map, with $4\times$ the weight in the regions excluding the nucleus (LH only).

^cIonization potential of contributing ion, or excitation temperature of upper level state (H_2).

ing of PDR heating processes (we note similar problems for H_2 and CO rotational emission observed in dense, warm Galactic PDRs, see Hollenbach & Tielens 1999), or a contribution of shock heating to the H_2 emission.

Also of note is the weak but well-detected $[\text{O IV}]$ line near $26\,\mu\text{m}$ (see Fig. 5). Lutz et al. (1998) found that $[\text{O IV}]$, with its high ionization potential of 55 eV, was nonetheless nearly universally present as weak emission in galaxies classified as starbursts from the relative strength of their $7.7\,\mu\text{m}$ PAH features. The O^{3+} ionization potential is just above the He^+ Lyman limit of 54.4 eV, and as a result $[\text{O IV}]$ is rarely formed in H II re-

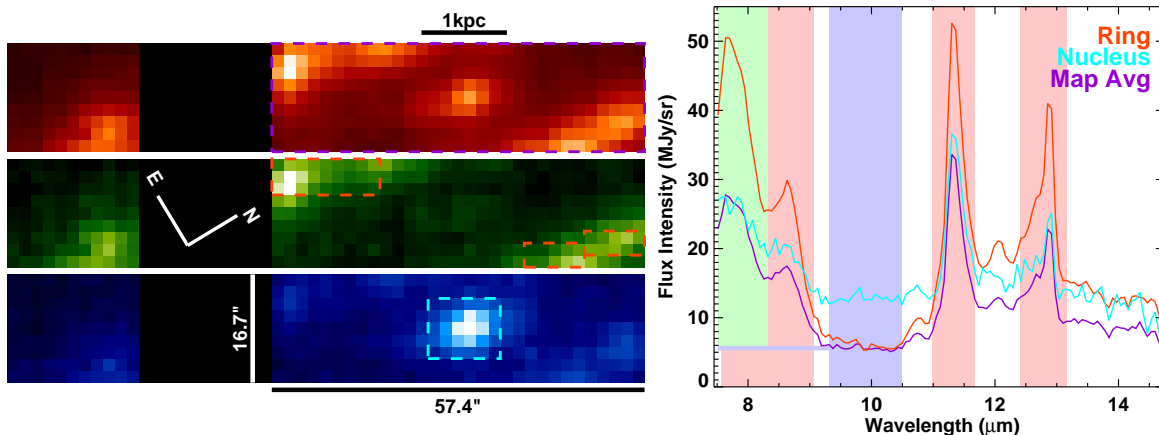


FIG. 4.— Three maps created by summing over the SL order 1 (7.5–14.7 μm) spectral cube, covering the nuclear and a portion of the flanking regions illustrated in Fig. 1, are shown at top. In red (top panel), a sum of the main PAH features at 7.7, 8.6, 11.3 and 12.7 μm ; in green (second panel), the continuum-subtracted 7.7 μm PAH feature map; and in blue (third panel) a pure continuum map centered at 10 μm . The colored shading in the plot below illustrates the spectral regions which were used to create the three maps, including 10 μm continuum subtraction in the 7.7 μm map. The spectra (bottom panel), show three separate extractions in different regions outlined with dashed lines in the maps: an average spectrum over the nucleus and ring (purple, lowest curve), a ring-only spectrum (orange, highest curve), and a nuclear spectrum (cyan, middle curve).

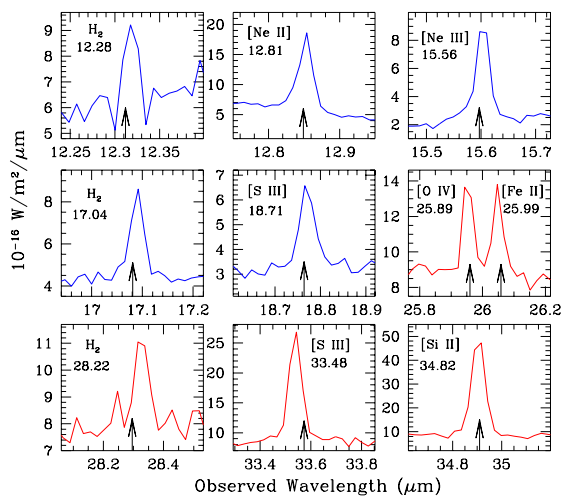


FIG. 5.— Emission lines from the SH and LH spectra extracted from the inner nuclear regions (blue and red outlined) indicated in Fig. 1. Some residual wavelength calibration offsets in the pipeline are evident.

gions. Any observed [O IV] therefore requires shocks, the wind-enhanced far-ultraviolet emission of Wolf–Rayet stars, or an AGN, to provide sufficient high energy photons (e.g. Schaerer & Stasińska 1999).

When the $[\text{O IV}]/([\text{Ne III}] + 0.44 [\text{Ne II}])$ ratio (O^{3+} to emissivity-weighted neon emission) is compared to the excitation measure $[\text{Ne III}]/[\text{Ne II}]$ (as in Lutz et al. (1998) Fig. 2), NGC 7331 is found to lie well above the locus of starburst galaxies, with [O IV] emitting more than 12% of the weighted neon line flux (vs. 1% typical for traditional starbursts). That [O IV] is centrally concentrated is evident from the relative line intensity in the inner to outer map. Both the relative strength and tight spatial distribution of [O IV] support the conclusion that a weak AGN provides the ionizing source, though a central concentration of high-mass stars cannot be ruled out.

The AGN hypothesis is given further credence by noting that preliminary HST Paschen- α imaging of the center of NGC 7331 indicates little or no atomic hydrogen line emission from the nucleus (D. Calzetti et al. 2004, in prep.).

4. CONCLUSIONS

All IRS modules were used to map the inner ~ 5 kpc of the nearby spiral galaxy NGC 7331. A new band feature at 17.1 μm , associated with the 16.4 μm PAH feature observed in Galactic nebulae, was found at 49% of the 11.3 μm PAH strength, making it an important contributor to the total MIR flux. Among the 7 detected fine structure lines was [O IV], whose strength and central concentration indicate an AGN or an unusual concentration of massive stars as the ionizing source. Two [S III] fine structure lines fix the typical pressure in H II regions to be $p/k \lesssim 4 \times 10^6 \text{ cm}^{-3} \text{ K}$, and the three H_2 rotational lines require that the bulk of the non-ionizing stellar radiation be processed through PDRs with similar pressures. The traditional PAH features at 7.7 and 11.3 μm were found to vary in strength, with the nucleus maintaining strong 11.3 μm emission relative to 7.7 μm .

The authors thank J. Houck, V. Charmandaris, and the IRS team for calibration and validation assistance, and K. Sellgren for discussion of NGC 7023's PAH features. It is also a pleasure to thank the SINGS liaison scientist, N. Silbermann, and the other members of the SSC staff for their support during the planning and execution of these observations. Support for this work, part of the *Spitzer Space Telescope* Legacy Science Program, was provided by NASA through Contract #1224769 issued by JPL/Caltech under NASA contract 1407.

REFERENCES

- Allamandola, L. J., & Hudgins, D. M. 2003, in *Solid State Astrochemistry*, 251
- Draine, B. T., & Bertoldi, F. 2001, in *Molecular H₂ in Space*, 131

- Filho, M. E., Barthel, P. D., & Ho, L. C. 2002, *ApJS*, 142, 223
Genzel, R., et al. 1998, *ApJ*, 498, 579
Helou, G., Malhotra, S., Hollenbach, D. J., Dale, D. A., & Contursi, A. 2001, *ApJ*, 548, L73
Hollenbach, D., & Tielens, A. 1999, *Rev. Mod. Phys.*, 71, 173
Houck, J. R., et al. 2004, *ApJS*
Kennicutt, R. C., et al. 2003, *PASP*, 115, 928
Li, A., & Draine, B. T. 2001, *ApJ*, 554, 778
Lutz, D., Kunze, D., Spoon, H. W. W., & Thornley, M. D. 1998, *A&A*, 333, L75
Moutou, C., Verstraete, L., Léger, A., Sellgren, K., & Schmidt, W. 2000, *A&A*, 354, L17
Pagani, L., et al. 1999, *A&A*, 351, 447
Regan, M. W., et al. 2004, *ApJS*, 154
Sanders, D. B., & Mirabel, I. F. 1996, *ARA&A*, 34, 749
Schaerer, D., & Stasińska, G. 1999, *A&A*, 345, L17
Smith, B. J. 1998, *ApJ*, 500, 181
Sturm, E., et al. 2002, *A&A*, 393, 821
Thornley, M. D., et al. 2000, *ApJ*, 539, 641
Werner, M. W., et al. 2004, *ApJS*, 154